Adjustment of Stratified Flow over a Sloping Bottom*

DAVID C. CHAPMAN AND STEVEN J. LENTZ

Woods Hole Oceanographic Institution, Woods Hole, Massachusetts

(Manuscript received 9 January 1996, in final form 5 August 1996)

ABSTRACT

The evolution of a steady stratified along-isobath current flowing cyclonically (shallower water on the right looking downstream) over a sloping frictional bottom is examined using an idealized model. The flow is assumed to consist of an inviscid vertically uniform geostrophic interior above a bottom boundary layer in which density is vertically well mixed. Within the bottom boundary layer, vertical shear in the horizontal velocities is assumed to result only from horizontal density gradients. Density advection is included in the model, but momentum advection is not. The downstream evolution of the current is described by two coupled nonlinear partial differential equations for surface pressure and boundary layer thickness, each of which is first order in the along-isobath coordinate and can be easily integrated numerically.

An initially narrow along-isobath current over a uniformly sloping bottom spreads and slows rapidly owing to the effects of bottom friction, much like the unstratified case. However, as the bottom boundary layer grows, the resulting horizontal density gradients reduce the bottom velocity, which in turn, decreases both the transport in the bottom boundary layer and the spreading of the current. An equilibrium is reached downstream in which the bottom velocity vanishes everywhere and the current stops spreading. This equilibrium flow persists indefinitely despite the presence of a frictional bottom. The width of the equilibrium current scales as $W \sim (f/N\alpha)(F_0/f)^{1/2}$, where f is the Coriolis parameter, N the buoyancy frequency, α the bottom slope, and F_0 the inflow volume flux per unit depth. The thickness of the bottom boundary layer scales as αW, while the along-isobath velocity scales as $(N\alpha/f)(F_0 f)^{1/2}$. Surprisingly, the downstream equilibrium flow is independent of the magnitude of bottom friction. Good approximations for the equilibrium scales are obtained analytically by imposing conservation of mass and buoyancy transports. Generalizations to variable bottom slope, nonuniform stratification, and coastal currents are also presented.

1. Introduction

Low-frequency or quasi-steady ocean currents in contact with the bottom tend to flow cyclonically along local isobaths (i.e., with shallower water on the right in the Northern Hemisphere). This is not surprising because long topographic Rossby waves propagate in this sense, so information is naturally transmitted in this direction. What is remarkable about many along-isobath currents is their persistence; that is, their narrow structure often continues for many hundreds of kilometers, apparently with little change in form or water properties. Examples include long coastal currents like that on the eastern North American shelf, slope currents such as the Labrador and East Greenland Currents, poleward undercurrents along some continental slopes, deep western boundary currents, and some deep flows along abyssal ridges. The persistence of such flows is surprising because an along-isobath flow in contact with the bottom ought to experience frictional drag, which should generate an Ekman-like bottom boundary layer with a cross-isobath component of transport, which in turn, should spread and decelerate the flow. One does not, therefore, expect a flow to remain narrow and distinct over a long distance.

The combination of ambient stratification and a sloping bottom complicates this simple logic because transport in the bottom boundary layer may redistribute buoyancy. For example, the cross-isobath transport in the bottom boundary layer beneath a cyclonic along-isobath flow is directed toward deeper water. In a stably stratified fluid, this produces a downslope buoyancy flux in which less dense water is carried under denser water. The water column becomes unstable and must overturn and mix, creating a rapidly thickening bottom boundary layer with horizontal density gradients. (This is sometimes called a downwelling-favorable flow by analogy to the coastal process of wind-driven downwelling.) The horizontal density gradients within the bottom boundary layer then lead (through thermal wind) to vertical shear of the along-isobath current. The vertical shear modifies the along-isobath current that drives the bottom bound-

* Woods Hole Oceanographic Institution Contribution Number 9182

Corresponding author address: Dr. David C. Chapman, Woods Hole Oceanographic Institution, Woods Hole, MA 02543.
E-mail: dchapman@whoi.edu.

ary layer. So, the redistribution of buoyancy modifies both the bottom boundary layer flow and the along-isobath flow above it. The behavior of both flows is no longer obvious, raising the basic question of how a stratified along-isobath flow adjusts over a sloping bottom.

A number of recent studies have begun to investigate this issue by examining the development of the bottom boundary layer beneath a stratified flow and its potential impact on the overlying flow (see the excellent review by Garrett et al. 1993). In particular, Trowbridge and Lentz (1991) and MacCready and Rhines (1993) developed one-dimensional models of boundary layer growth normal to a uniformly sloping bottom in a semi-infinite fluid. They showed that one of the primary effects of vertical shear in the bottom boundary layer associated with the horizontal density gradient is to reduce the stress at the bottom. As the boundary layer grows, the bottom stress and, consequently, the cross-isobath buoyancy flux both decrease. Eventually, a steady state is approached in which the bottom stress and buoyancy flux become negligible, so the bottom appears slippery to the overlying flow. The implication is that the overlying flow could continue indefinitely, unimpeded by bottom friction.

These recent results suggest a basic mechanism that may contribute to the persistence of narrow ocean currents. However, one-dimensional models are not adequate to address the three-dimensional evolution of a spatially varying stratified flow that adjusts to an evolving bottom boundary layer. For example, the initial flow in the models of Trowbridge and Lentz (1991) and MacCready and Rhines (1993) is spatially uniform, extending to infinity away from and along the bottom. As the bottom boundary layer develops, the overlying flow (above the bottom boundary layer) remains fixed at its initial value; that is, it is constant in both space and time. Thus, the development of the bottom boundary layer alters the overlying flow only within the boundary layer itself. There is no feedback between the boundary layer flow and the overlying flow. In contrast, spatial variations in the initial flow (e.g., a narrow current) create spatial variations in boundary layer growth with associated regions of convergence and divergence in the bottom boundary layer. The initial current must adjust to these variations in the bottom boundary layer, so the overlying flow must change. An altered overlying flow affects the growth of the bottom boundary layer, and so on. One-dimensional models cannot account for this feedback.

The goal of this work is to examine the evolution and adjustment of a stratified along-isobath flow over a sloping frictional bottom in which feedback between the bottom boundary layer and the overlying flow can occur. The emphasis is on understanding the basic dynamics that allow narrow currents to persist over long distances in the ocean. To this end, an idealized model is constructed in section 2, the general behavior of which is discussed in section 3. Scalings are introduced in section 4 to simplify the presentation of results. The adjustment of a narrow current over a uniform slope with initially uniform stratification is described in section 5. The behavior of the flow far downstream from the source is examined in section 6. Generalizations to variable bottom slope, variable stratification, and coastal flows are presented in section 7. Some implications of the results are discussed in section 8, followed by concluding remarks in section 9.

2. Model formulation

Steady hydrostatic flow of a stratified fluid over a sloping bottom is considered. Bottom topography varies only in the y direction; that is, the x axis is everywhere parallel to the isobaths. Momentum advection is neglected, but density advection is included. The along-isobath scale of the flow is assumed to be much larger than the cross-isobath scale, rendering the along-isobath flow in geostrophic balance. Lateral diffusion of both momentum and density is neglected. The momentum, continuity, and density equations may be written as

$$-fv = -p_x/\rho_0 + \tau^x_z/\rho_0 \tag{1}$$

$$fu = -p_y/\rho_0 \tag{2}$$

$$0 = p_z + g\rho \tag{3}$$

$$u_x + v_y + w_z = 0 \tag{4}$$

$$u\rho_x + v\rho_y + w\rho_z = B_z, \tag{5}$$

where (u, v, w) are the velocity components in the along-isobath (x), cross-isobath (y), and vertical (z) directions, respectively; p is pressure; ρ is the density anomaly relative to the constant surface density ρ_0; f is the Coriolis parameter; τ^x is the stress in the along-isobath (x) direction; B is the vertical turbulent density flux; and g is gravitational acceleration. Subscripts x, y, and z denote partial differentiation. For convenience, the density anomaly ρ is referred to as the density.

The flow is confined between the surface at $z = 0$ and the bottom at $z = -h(y)$. It is assumed to consist of two distinct regions: a bottom boundary layer of thickness $\delta(x, y)$ and an interior extending from the top of the bottom boundary layer to the surface (Fig. 1). The interior flow is inviscid, vertically uniform, and free of mixing, that is, no stress ($\tau^x = 0$), no vertical shear ($\partial/\partial z = 0$), and no density flux ($B = 0$). Isopycnals are, therefore, always horizontal in the interior. Mixing is confined to the bottom boundary layer and is strong enough to mix density completely in the vertical. Thus, isopycnals are vertical in the bottom boundary layer, while horizontal density gradients and associated thermal-wind vertical shears may be present. The implicit assumption is that the boundary layer thickness is large enough that most of the shear is produced by the horizontal density gradients and not the stress at the bottom. This situation is approached fairly rapidly in the one-

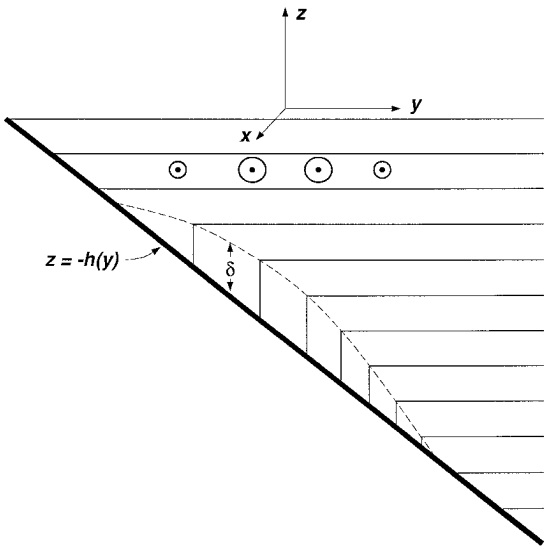

FIG. 1. Model geometry and stratification. An along-isobath flow toward $+x$ (represented by circles) over a sloping bottom, $z = -h(y)$, adjusts in the presence of a growing bottom boundary layer of thickness δ. The interior, above the bottom boundary layer, is inviscid and vertically stratified, while density in the bottom boundary layer is completely mixed in the vertical. Isopycnals are continuous across the top of the bottom boundary layer.

dimensional model of MacCready and Rhines (1993). Finally, isopycnals are assumed to be continuous across the top of the bottom boundary layer, so the density at the bottom is simply the vertical projection of the density at the top of the bottom boundary layer down to the bottom.

Restating mathematically, using (1)–(4), the two regions have the following properties:

Interior $-h + \delta < z \le 0$;

$$\begin{aligned} &\rho_x = \rho_y = 0, \qquad \rho_z = -\rho_0 N^2 \Gamma'(z)/g \\ &p_x = p^s_x, \qquad p_y = p^s_y \\ &u^i = -p^s_y/\rho_0 f, \qquad v^i = p^s_x/\rho_0 f, \qquad w^i = 0. \end{aligned} \tag{6}$$

Bottom boundary layer $-h \le z \le -h + \delta$;

$$\begin{aligned} &\rho_z = 0 \\ &p_x = p^s_x + g\rho_x(\delta - h - z), \\ &p_y = p^s_y + g\rho_y(\delta - h - z), \\ &u = -[p^s_y + g\rho_y(\delta - h - z)]/\rho_0 f \\ &\quad = u^i - g\rho_y(\delta - h - z)/\rho_0 f, \end{aligned} \tag{7}$$

where p^s is the surface pressure, N is the buoyancy frequency at $z = 0$, $\Gamma(z)$ is the vertical structure of the interior density, and the prime indicates the derivative with respect to the argument. The function $\Gamma(z)$ is chosen to increase with depth from zero at $z = 0$, with its derivative equal to unity at $z = 0$. For example, uniform stratification corresponds to $\Gamma(z) = z$. Note that the vertical structures of v and w in the bottom boundary layer are unknown because the vertical structure of τ^x_z is not specified.

In keeping with the assumed interior flow, no density flux or stress is applied at the surface:

$$B = \tau^x = 0 \qquad z = 0.$$

At the bottom, there is no density flux and the stress is assumed proportional to the velocity:

$$B = 0, \ \tau^x/\rho_0 = ru \qquad z = -h,$$

where r is a bottom friction coefficient. No flow is permitted through either the surface or the bottom:

$$\begin{aligned} w &= 0 \qquad z = 0 \\ w &= -vh_y \qquad z = -h. \end{aligned}$$

The momentum equations (1) and (2) and continuity (4) may be integrated vertically, making use of (6) and (7) and the boundary conditions, to obtain

$$-fV = -\frac{1}{\rho_0}p^s_x - \frac{g}{2\rho_0 h}\delta^2\rho^b_x - \frac{r}{h}u^b \tag{8}$$

$$fU = -\frac{1}{\rho_0}p^s_y - \frac{g}{2\rho_0 h}\delta^2\rho^b_y \tag{9}$$

$$(Uh)_x + (Vh)_y = 0, \tag{10}$$

where $(U, V) = h^{-1}\int_{-h}^{0}(u, v)\,dz$ are the depth-averaged velocities, and u^b and ρ^b are the along-isobath velocity and density, evaluated at the bottom, $z = -h$. From (7),

$$u^b = -(p^s_y + g\rho^b_y\delta)/\rho_0 f = u^i - g\rho^b_y\delta/\rho_0 f. \tag{11}$$

Combining (8)–(10) to eliminate the depth-averaged velocities and using (11) produces

$$p^s_x - \frac{r}{fh_y}p^s_{yy} = \frac{g}{h_y}\left[\frac{r}{f}(\delta\rho^b_y)_y + \delta(\rho^b_y\delta_x - \rho^b_x\delta_y)\right]. \tag{12}$$

In terms of p^s, (12) looks like a one-dimensional diffusion or heat equation, forced by a function depending on the thickness of the bottom boundary layer and the density gradients therein. The along-isobath direction x takes the place of time; that is, the evolution of surface pressure along the isobaths is analogous to the evolution of temperature with time for the heat equation. In fact, in the absence of stratification ($\rho^b_x = \rho^b_y = 0$), the right-hand side of (12) vanishes, reducing it to the arrested topographic wave model constructed by Csanady (1978) for which the heat equation analogy has been used quite successfully for years. Alternatively, Csanady's model may be recovered by setting $\rho^b_x = \rho^b_y = 0$ and $u^b = U$ in (8)–(10). However, as shown below, the right-hand side of (12) is a function of p^s and, therefore, cannot be viewed simply as a forcing term for p^s. Rather, the right-hand side of (12) represents feedback between the bottom boundary layer and the interior flow.

Another equation relating δ, ρ^b, and p^s may be obtained by vertically integrating the density equation (5). The interior flow contributes nothing to the integral, so this is equivalent to integrating vertically through the bottom boundary layer, $\int_{-h}^{-h+\delta} dz$. Furthermore, the vertical advection and diffusion terms, $w\rho_z$ and B_z, contribute nothing because $\rho_z = 0$ in the bottom boundary layer and $B = 0$ at the bottom and at the top of the bottom boundary layer. Noting that ρ_x and ρ_y are independent of z within the bottom boundary layer and using (1), (7), and the bottom stress condition yields

$$\rho_x^b \delta f u^i + \rho_y^b (r u^b + \delta f v^i) = 0. \tag{13}$$

The cross-isobath buoyancy flux in the bottom boundary layer is assumed to be dominated by the bottom stress associated with the along-isobath velocity, so the contribution from the interior cross-isobath velocity $\delta f v^i$ is neglected in (13) to obtain

$$\rho_x^b \delta = -\rho_y^b \frac{r u^b}{f u^i}. \tag{14}$$

The validity of this assumption is discussed further in section 8.

The remaining step is to relate the bottom boundary layer thickness to the bottom density. The density within the bottom boundary layer is simply the density at the top of the boundary layer; that is, $\rho^b = \rho|_{z=-h+\delta}$, which from (6) becomes

$$\rho^b = -\frac{\rho_0 N^2}{g} \Gamma|_{z=-h+\delta}. \tag{15}$$

For example, uniform stratification ($\Gamma = z$) yields $\rho^b = -\rho_0 N^2(\delta - h)/g$. Substitution of (15) into (12) and (14) results in

$$p_x^s - \frac{r}{f h_y} p_{yy}^s = \rho_0 N^2 \left\{ \frac{r}{f h_y} [(h_y - \delta_y)\delta \Gamma']_y + \frac{\Gamma'}{2} (\delta^2)_x \right\} \tag{16}$$

$$(\delta^2)_x = 2(h_y - \delta_y) \frac{r u^b}{f u^i} \tag{17}$$

with

$$u^b = u^i - N^2 (h_y - \delta_y) \delta \Gamma' / f \tag{18}$$

$$u^i = -p_y^s / \rho_0 f, \tag{19}$$

where Γ' here means $d\Gamma/dz$ evaluated at $z = -h + \delta$. The physical behavior encompassed by these equations is discussed in section 3.

Three lateral boundary conditions are required for both p^s and δ (one in x and two in y). The condition in x consists of a specified along-isobath inflow with no bottom boundary layer at $x = 0$. In the absence of physical lateral boundaries, the inflow $x = 0$ is chosen as at

$$u^i = \begin{cases} u_0 = -p_y^s/\rho_0 f, & -W_0 \le y \le W_0 \\ 0, & y < -W_0,\ y > W_0 \end{cases} \tag{20}$$

$$\delta = 0, \qquad \text{all } y, \tag{21}$$

where u_0 is the inflow velocity and W_0 is the half-width of the inflow. In this case, the along-isobath velocity and the bottom boundary layer thickness should vanish away from the current, so

$$u^i = -p_y^s \to 0 \text{ and } \delta \to 0, \qquad y \to \pm\infty.$$

For coastal flows, a solid boundary is imposed at $y = 0$ with zero transport normal to the boundary. From (8), using (15) and (18), the coastal boundary condition is

$$p_x^s - \frac{r}{f h_c} p_y^s = \frac{\rho_0 N^2 \Gamma'}{h_c} [r(h_y - \delta_y)\delta/f + \delta_x \delta^2/2] \qquad y = 0, \tag{22}$$

where h_c is the depth at the coast and Γ' again means $d\Gamma/dz$ evaluated at $z = -h + \delta$. In this case, the inflow condition is modified such that u_0 is applied only for $y > 0$, and u^i, $\delta \to 0$ at $y \to +\infty$.

The nonlinear system defined by (16)–(19) appears to preclude analytical solutions, so a numerical approach is taken here. The occurrence of only first derivatives in x suggests that (16)–(19) may be integrated numerically starting from the specified initial state at $x = 0$. The lateral boundary conditions at $y \to \pm\infty$ are approximated by

$$p_y^s = \delta = 0 \qquad y = \pm W_\infty, \tag{23}$$

where W_∞ is some large distance. To monitor the accuracy of the solution, the total along-isobath transport is computed at several x locations to be sure that mass is conserved. In all cases presented here, the space step in x has been adjusted to ensure mass conservation to within 0.2% of the specified inflow.

The model is completely specified by choosing the topography $h(y)$, bottom friction coefficient r, buoyancy frequency at the surface N, density structure $\Gamma(z)$, Coriolis parameter f, and the appropriate boundary conditions. The model is physically well posed, but two constraints must be imposed in the numerics to ensure solutions consistent with the model assumptions. Both are implicit in the model derivation. First, the bottom boundary layer cannot grow thicker than the total water depth; that is, δ must remain less than h. This is not an issue for most of the calculations presented below, being invoked only close to the coast in some coastal flows (section 7). Second, the assumed structure of the flow (Fig. 1) implies that the bottom boundary layer can only grow and cannot shrink because there is no mechanism to restratify the water column. Therefore, δ can only increase or remain constant as x increases. This is not a problem provided the initial state at $x = 0$ is limited to cyclonic flows, that is, toward $+x$, which are expected to lead to a density structure like that in Fig. 1.

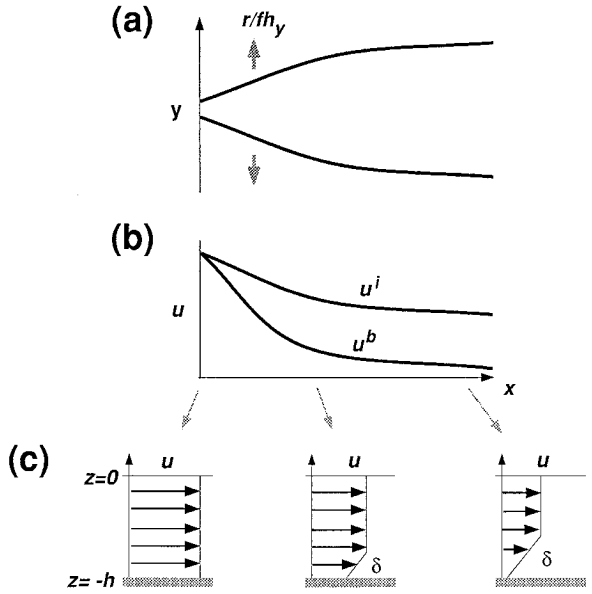

FIG. 2. Schematic depicting the adjustment and evolution of a narrow inflow starting at $x = 0$. (a) Plan view of the current boundaries that initially spread, owing to bottom friction, at a rate set by r/fh_y. (b) Evolution of the interior velocity u^i and bottom velocity u^b with downstream distance. (c) Along-isobath velocity profiles at various stages downstream. The bottom boundary layer grows, while the interior and bottom velocities both decrease, eventually reaching an equilibrium where the bottom velocity vanishes.

3. Preliminaries: General model behavior

Before launching into a presentation of model solutions, it is useful to anticipate model behavior by examining some features of the model equations (16)–(19). As mentioned above, the right-hand side of (16) vanishes in the absence of stratification (i.e., $N = 0$), and the model reduces to the arrested topographic wave model derived by Csanady (1978). There is no buoyancy to redistribute, so (16) and (17) are uncoupled. In this case, the left-hand side of (16) describes the spreading of an along-isobath current by cross-isobath transport in the bottom Ekman layer. The rate of spreading with downstream distance is set by r/fh_y, the effective ''diffusivity'' by analogy to the heat equation, and thus increases with stronger bottom friction, gentler bottom slope and/or slower rotation rate. The spreading of an initially narrow current is depicted schematically in Fig. 2a.

In the presence of stratification, the bottom boundary layer redistributes buoyancy by growing beneath the along-isobath flow, developing a structure like that in Fig. 1. In this case, (16) and (17) are coupled; that is, there is feedback between the bottom boundary layer and the interior flow. The bottom boundary layer changes thickness in response to the interior flow, through (17)–(19), which then alters the spreading and structure of the interior, through (16). The altered interior flow, in turn, alters the growth of the bottom boundary layer, and so on. The strength of the feedback [right-hand side of (16)] is proportional to N^2; that is, stronger interior stratification amplifies the effect of the bottom boundary layer on the interior flow. Thus, the adjustment of the interior flow and the growth of the bottom boundary layer should occur over shorter horizontal scales when the background stratification is stronger.

The bottom boundary layer will grow wherever the right-hand side of (17) is positive. The assumed initial state (at $x = 0$) is a cyclonic flow with no bottom boundary layer, that is, $\delta = \delta_y = 0$ and $u^b = u^i > 0$; so the bottom boundary layer initially grows. As the bottom boundary layer thickens downstream, the bottom velocity u^b decreases relative to the interior velocity u^i according to (18), as depicted schematically in Fig. 2. Reduced u^b slows the growth of the bottom boundary layer in (17). If the bottom boundary layer ever becomes thick enough to reduce the bottom velocity to zero in (18), that is, $u^b \to 0$, then boundary layer growth ceases according to (17). However, the right-hand side of (16) does not vanish in this case, so the coupling between the interior flow and the bottom boundary layer remains. If, in addition, the cross-isobath velocity vanishes (i.e., $v^i = p_x^s/\rho_0 f \to 0$), then there exists the possibility of a downstream equilibrium state in which $u^b = 0$ everywhere. Where this occurs, if at all, depends on the adjustment of the interior flow and cannot be simply determined a priori.

The bottom boundary layer may also stop growing if its top becomes horizontal in the cross-isobath direction, that is, $h_y - \delta_y = 0$, which reduces the right-hand side of (17) to zero. In this case, the top of the bottom boundary layer is coincident with an interior isopycnal, so the cross-isobath density gradient vanishes within the bottom boundary layer. According to (18), the vertical shear in the along-isobath flow vanishes as well, so $u^b = u^i$. With $(\delta^2)_x = 0$ and $h_y - \delta_y = 0$, the entire right-hand side of (16) disappears, and the model locally reduces to the arrested topographic wave, despite the presence of interior stratification. The implication is that the bottom boundary layer cannot grow beyond the point where $h_y - \delta_y = 0$, a situation which may be approached at the shallow edge of the bottom boundary layer (Fig. 1).

Bottom friction takes on two competing roles in (16)–(19). On one hand, bottom friction is responsible for spreading the flow [left-hand side of (16)], so an increase in r leads to a wider, slower flow. On the other hand, the growth of the bottom boundary layer in (17) is proportional to the strength of bottom friction; that is, boundary layer growth increases as r increases. A faster growing bottom boundary layer reduces the bottom stress more rapidly, thereby reducing the spreading of the flow. Therefore, strong bottom friction (large r) leads to rapid spreading but also to rapid reduction in bottom stress that reduces spreading. Weak bottom friction (small r) leads to slow spreading but also slow boundary layer growth, so the flow may spread more

before the boundary layer grows enough to reduce the bottom stress to zero. This behavior suggests that the two effects may tend to compensate, and any equilibrium state achieved far downstream may be insensitive to the strength of bottom friction.

The bottom slope also affects both spreading and boundary layer growth, but in ways that reinforce each other. A steeper bottom slope leads to less spreading by decreasing r/fh_y on the left-hand side of (16). From (17) and (18), a steeper bottom slope also leads to faster growth of the bottom boundary layer and increased shear in the bottom boundary layer, both of which decrease the bottom velocity more rapidly with a consequent reduction in spreading. Thus, a steeper bottom slope should produce a narrower, stronger current.

Two other points are worth noting here: First, the total depth h appears in (16)–(19) only through Γ'. For uniform stratification, $\Gamma' = 1$ and the solution is independent of the total depth. The topography then enters only through the bottom slope (and the depth at the coast for coastal flows). Second, if three conditions are satisfied, namely, 1) the boundary layer thickness and bottom slope are independent of the cross-isobath coordinate ($\delta_y = 0$ and $h_y = \alpha$), 2) stratification is uniform ($\Gamma' = 1$), and 3) the bottom velocity vanishes ($u^b = 0$), then (18) reduces to $\delta = fu^i/\alpha N^2$, which is identical to the one-dimensional model result of Trowbridge and Lentz [1991; their equation (31) after an appropriate change of coordinates]. This limit is contrasted with the downstream equilibrium solution of (16)–(19) in section 4.

4. Scaling

An appropriate choice of scaling can both simplify the model equations (16)–(19) and provide information about the relative sizes of terms and the dependence of model variables on model parameters. First, the inflow is assumed to adjust over a cross-isobath scale W. An appropriate along-isobath length scale L can then be obtained by making both terms on the left-hand side of (16) order one. An appropriate vertical scale is αW where α is a typical bottom slope. Using these length scales, an along-isobath velocity scale is found from (18). The pressure scale follows from geostrophy in (6), which then determines the cross-isobath velocity scale as well. Accordingly, model variables are scaled as

$$\begin{aligned} y &\quad \text{by } W \\ x &\quad \text{by } L = f\alpha W^2/r \\ h,\delta &\quad \text{by } \alpha W \\ u &\quad \text{by } N^2\alpha^2 W/f \\ v &\quad \text{by } N^2\alpha r/f^2 \\ p^s &\quad \text{by } \rho_0 N^2\alpha^2 W^2. \end{aligned} \tag{24}$$

With these scales (16)–(19) reduce to

$$p^s_x - \frac{1}{h_y}p^s_{yy} = \frac{1}{h_y}[(h_y - \delta_y)\delta\Gamma']_y + \frac{\Gamma'}{2}(\delta^2)_x \tag{25}$$

$$(\delta^2)_x = 2(h_y - \delta_y)\frac{u^b}{u^i} \tag{26}$$

$$u^b = u^i - (h_y - \delta_y)\delta\Gamma' \tag{27}$$

$$u^i = -p^s_y \tag{28}$$

in which all variables are now nondimensional. This scaling eliminates all model parameters, so once h_y, Γ, and the inflow are specified, a single solution to (25)–(28) describes the result for all other parameter choices.

The cross-isobath scale W is determined by the inflow transport. The dimensional inflow transport is F_0h_0, where $F_0 = 2u_0W_0$ is the unscaled inflow volume flux per unit depth. Scaling u_0 and W_0 as in (24) and setting the nondimensional inflow volume flux per unit depth equal to unity leads to

$$F_0 = N^2\alpha^2W^2/f.$$

Solving for W yields

$$W = \left(\frac{f}{N\alpha}\right)\left(\frac{F_0}{f}\right)^{1/2}. \tag{29}$$

The cross-isobath adjustment scale is proportional to the square root of the inflow volume flux per unit depth and varies inversely with the Burger number, $N\alpha/f$. As the relative importance of stratification increases (decreases), the adjustment scale decreases (increases). For unstratified inflows $N \to 0$, so $W \to \infty$; that is, there is no limit to the spreading across isobaths, a result consistent with the arrested topographic wave model.

It is useful to reconsider the validity of some model assumptions in light of the scaling (24). The neglect of momentum advection in (1) and (2) is valid provided that the Rossby number is small; that is, $u/fW \ll 1$, which from (24) is $(N\alpha/f)^2 \ll 1$. That is, the square of the Burger number must be small. This is a good assumption in most of the deep ocean and over most continental shelves. It may be violated over the shallowest parts of highly stratified continental slopes, typically near the shelf break. The assumption of geostrophy in the cross-isobath momentum equation (2) requires that $\tau^y_z/\rho_0 \ll fu$ in the unscaled equations. Using a linear bottom stress law, $\tau^y_z/\rho_0 \sim rv/\delta$, the requirement becomes $(r/f\alpha W)^2 \ll 1$, which is simply a restatement of the assumption that the along-isobath scale is much greater than the cross-isobath scale ($W^2 \ll L^2$). So, the chosen scaling is consistent with the neglect of stress in (2). Interestingly, the restriction $W^2 \ll L^2$ constrains the inflow volume flux per unit depth; $F_0 \gg r^2N^2/f^3$. This is basically a statement that the inflow transport must be strong enough for the alongshelf flow to dominate the cross-shelf flow.

As anticipated in section 3, the width scale (29) is independent of bottom friction. The bottom friction co-

efficient r appears only in the x and v scales. This means that the downstream distance over which adjustment occurs and the cross-isobath velocity associated with the adjustment each depend on bottom friction, but any equilibrium state that develops far downstream and is independent of x (and, therefore, $v^i = p^s_x/\rho_0 f = 0$) is also independent of bottom friction. This is a convenient result considering that r is probably the poorest known parameter in the model.

The bottom boundary layer thickness scale is independent of bottom slope; that is, $\alpha W = (f/N)(F_0/f)^{1/2}$ using (29). In contrast, the equilibrium boundary layer thickness reported by Trowbridge and Lentz (1991) from their one-dimensional model is $\delta = fu^i/\alpha N^2$ (in the present notation), which is clearly a function of bottom slope, becoming ever larger as the bottom slope decreases. Further, as mentioned in section 3, setting the bottom velocity to zero in (18) produces an equilibrium bottom boundary layer thickness identical to that of Trowbridge and Lentz (1991). This apparent contradiction is a consequence of the lack of feedback between the bottom boundary layer and the interior flow in the one-dimensional model of Trowbridge and Lentz (1991); that is, u^i is fixed in their model. In the present model, u^i varies with the scale given by (24). Substituting the u scale for u^i in the Trowbridge and Lentz (1991) expression produces $\delta = \alpha W$, in agreement with (24). Therefore, the equilibrium bottom boundary layer scale for three-dimensional flow may be very different from the scale for one-dimensional flow, especially over a very gently sloping bottom, because of the adjustment of the interior velocity in response to boundary layer growth.

Thus, the scalings in (24) and (29) provide considerable insight into the behavior of the model and also greatly simplify the model equations. Henceforth, all variables are scaled in this manner unless otherwise noted. This also means that the nondimensional inflow volume flux per unit depth is fixed at unity in order for (29) to apply.

5. Adjustment of a narrow current over a uniform slope

The simplest example that illustrates the basic behavior and dynamics of the model constructed in section 2 is the adjustment of a narrow along-isobath current over a uniformly sloping bottom in the presence of uniform stratification. That is, the model is simplified by choosing $h_y = 1$ and $\Gamma' = 1$ in (25)–(28), and the inflow is imposed over a small cross-isobath distance relative to the adjustment scale W (i.e., $W_0 \ll 1$).

The model solution for an inflow with half-width $W_0 = 0.1$ and inflow velocity $u_0 = 5$ is presented in Fig. 3. The inflow is centered at $y = 0$ on the left boundary ($x = 0$), and isobaths (not shown) are parallel to the x axis with the shallowest water at the bottom edge of each panel ($y = -1.5$). The inflow widens rapidly as it moves downstream. The outermost contours of surface pressure and along-isobath velocity approach $y = \pm 1$ by $x = 0.3$ (Figs. 3a,b). The cross-isobath velocity reflects this spreading, with positive v^i on the deep side of the inflow and negative v^i on the shallow side (Fig.

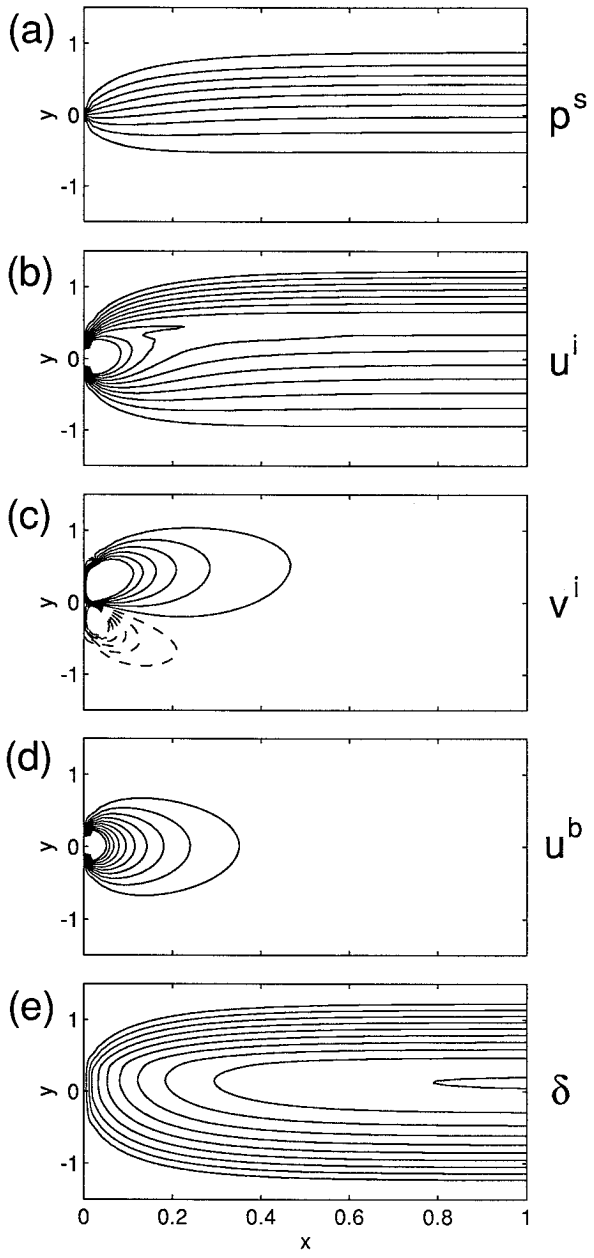

FIG. 3. Plan views of the adjustment of a narrow inflow over a uniformly sloping bottom with uniform initial stratification. The inflow enters at $x = 0$ between $y = \pm 0.1$. Shallower water is toward the bottom of each panel. Isobaths are parallel to the x axis. Variables are (a) surface pressure, (b) interior along-isobath velocity, (c) interior cross-isobath velocity, (d) bottom velocity, and (e) bottom boundary layer thickness. All variables are scaled according to (24). Contours are (a) 0.1 to 0.9 by 0.1, (b) 0.1 to 1 by 0.1, (c) −1.375 to 1.375 by 0.25, (d) 0.1 to 1 by 0.1, and (e) 0.06 to 0.6 by 0.06.

3c). The initial spreading may be understood by forming a vorticity equation from (8)–(10). Near $x = 0$, the bottom boundary layer has only begun to grow, so δ may be set to zero to obtain

$$-\frac{f\alpha}{h}V = \frac{\partial}{\partial y}\left(\frac{r}{h}u^b\right) \tag{30}$$

in which all variables are dimensional. Equation (30) expresses the balance between the stretching or squashing of a water column and Ekman pumping or suction in the bottom boundary layer, that is, the curl of the bottom stress. At $x = 0$, $u^b = u^i$, so the right-hand side of (30) is positive on the $-y$ side of the inflow, and V must be negative there. That is, water columns are squashed and must move toward shallower water. The reverse is true on the $+y$ side, so V is positive and flow is toward deeper water.

As the flow moves downstream, the bottom boundary layer grows beneath the along-isobath current (Fig. 3e). As expected, this rapidly reduces the bottom velocity (Fig. 3d), which, in turn, slows the spreading. By $x = 0.5$, the bottom velocity has nearly vanished, and the flow is approaching an equilibrium state independent of x. The cross-isobath velocity has nearly vanished as well. Beyond this point, the along-isobath current continues unchanged and unimpeded (Fig. 3b), despite the presence of a frictional bottom!

In terms of dimensional distances and velocities, the current adjustment depends on the various parameters that set the scales in (24) and (29). For example, stronger stratification, steeper bottom slope, or slower rotation rate each decreases W (and hence L), leading to a more rapid downstream adjustment (shorter x scale), a narrower equilibrium current, and larger along-isobath velocities. The opposite is true for weaker stratification, gentler bottom slope, and/or more rapid rotation rate. In the limit of vanishing stratification ($N \to 0$) the x and y scales become infinite, so the downstream equilibrium is never reached. This corresponds to Csanady's (1978) arrested topographic wave model described earlier and is shown for comparison in Fig. 4, the solution having been obtained by solving (25)–(28) with $\delta = 0$.[1] The scaling given by (24) is, of course, no longer valid because $N = 0$, so a quantitative comparison with Fig. 3 is not sensible. Nevertheless, the qualitative differences are clear even without specifying the scales. The surface pressure initially spreads rapidly across the isobaths with cross-isobath velocities that resemble those of the stratified model (Fig. 3). However, the spreading continues indefinitely in the downstream direction, never reaching a downstream equilibrium. The along-isobath velocity continues to widen and decrease downstream until, eventually, all signs of the inflow are lost. (This behavior may be obtained from Fig. 3, as well, by stretching both x and y axes to infinity as $W \to \infty$.)

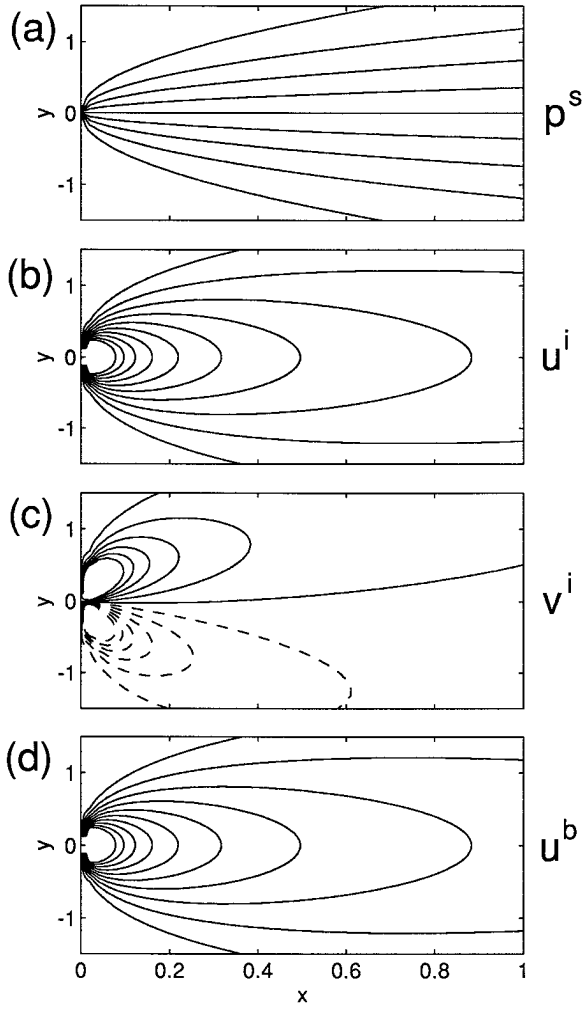

FIG. 4. As in Fig. 3 but for an unstratified flow. Note that $\delta = 0$, so panel (e) is not shown.

The along-isobath development of the bottom boundary layer thickness, the interior velocity, and the bottom velocity is presented in Fig. 5. The maximum value at each downstream location is plotted. The bottom boundary layer initially grows rapidly in the presence of stratification, but growth slows with distance downstream and approaches a maximum. The interior velocity decreases rapidly, then reaches a constant at $x \approx 0.2$. The bottom velocity continues to decrease downstream, vanishing by $x \approx 1$. The solution for the unstratified case (dashed curves) is shown for comparison simply to demonstrate that the unstratified solution never reaches an equilibrium but rather continues to decay downstream. As explained above, the comparison is only qualitative because the x scales for the two cases are different.

The downstream evolution of the dynamical balance is shown in Fig. 6 where each of the four terms in (25) is plotted on each side of the inflow ($y = \pm 0.33$). Near

[1] Remember that $\delta = 0$ here means no buoyancy flux in the bottom boundary layer, not a vanishing bottom Ekman layer.

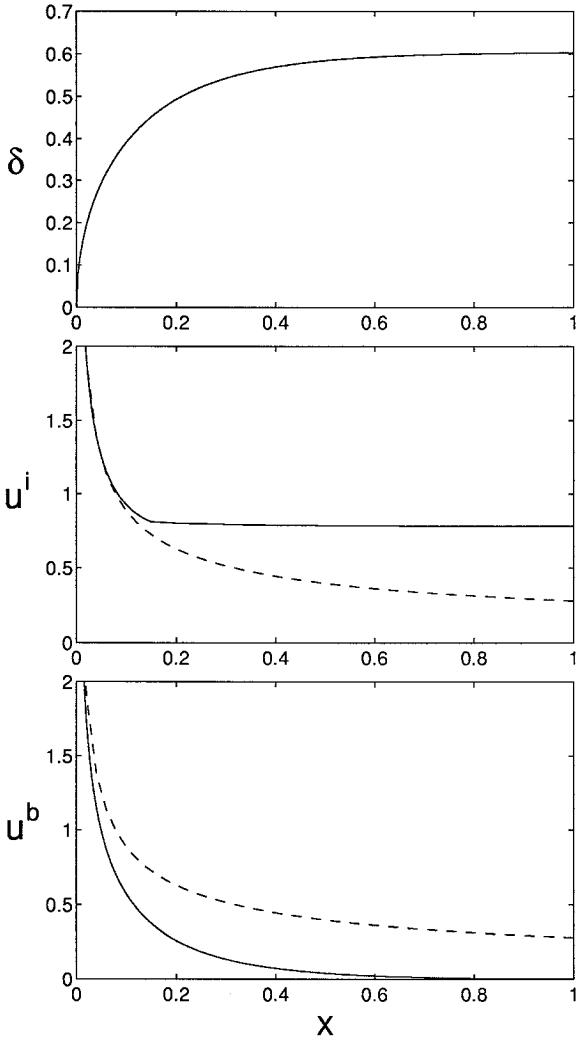

FIG. 5. Maximum values of (upper) bottom boundary layer thickness, (middle) interior along-isobath velocity, and (lower) bottom velocity at each downstream (x) location for the stratified flow shown in Fig. 3. Dashed curves correspond to the unstratified flow in Fig. 4.

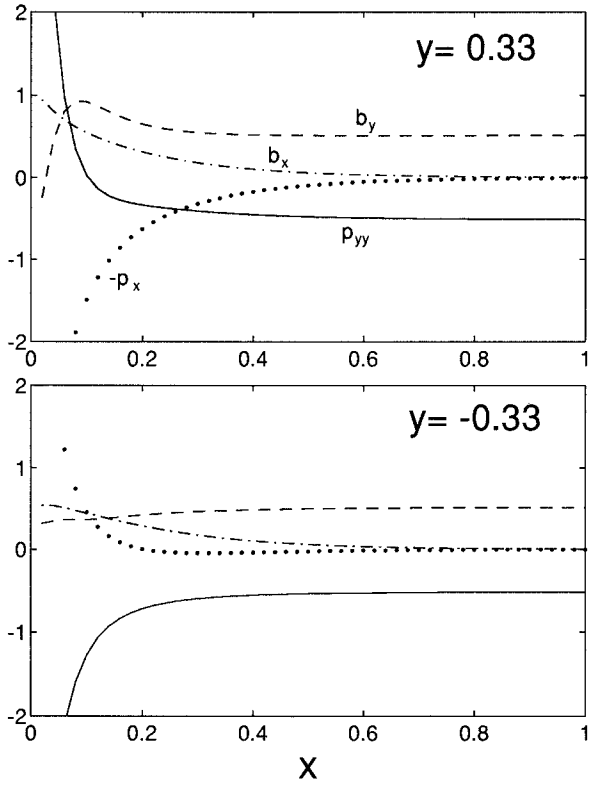

FIG. 6. Along-isobath evolution of the four terms in (25) at (upper) $y = 0.33$ and (lower) $y = -0.33$ for the stratified flow shown in Fig. 3. Solid curves are p^s_{yy}; dotted curves are $-p^s_x$; dashed curves are $b_y = h_y^{-1}[(h_y - \delta_y)\delta]_y$; dash-dotted curves are $b_x = \frac{1}{2}(\delta^2)_x$.

the inflow ($x < 0.2$), the dramatic adjustment is almost entirely associated with the spreading of the inflow. As mentioned above, the bottom boundary layer is quite thin in this region, so density effects (buoyancy forces) are minimal. The dynamical balance is essentially the arrested topographic wave, that is, $p^s_x \approx p^s_{yy}$. Bottom boundary layer growth, $b_x = (1/2)(\delta^2)_x$, is largest near the inflow (see also Fig. 5) and then decreases slowly downstream. Farther downstream, the along-isobath gradients decrease as the bottom boundary layer grows, leaving a balance between $-p^s_{yy}$ and $b_y = h_y^{-1}\,[(1 - \delta_y)\delta]_y$ in the equilibrium flow.

The along-isobath decay or shutdown scale over which the inflow approaches the downstream equilibrium state is L, given by (24). This scale is consistent with an estimate for a shutdown *time* scale made by Garrett et al. (1993) based on a one-dimensional model. They argued that the shutdown time for the bottom boundary layer is of order $(1/2)C_d^{-1}N^{-1}(f/N\alpha)^3$, where C_d is the drag coefficient in a quadratic drag law for bottom stress. This shutdown time scale may be converted to a shutdown length scale in the presence of a linear bottom stress law (as in the present model) by multiplying by an advective velocity u and setting $C_d = r/u$ to obtain

$$L^G \sim \frac{1}{2}(u^2/r)(f/N\alpha)^3 N^{-1}.$$

Using the u scale from (24), this becomes

$$L^G \sim \frac{1}{2} f\alpha W^2/r = \frac{1}{2}L.$$

Despite the consistency, neither scale agrees particularly well with the scale over which the bottom velocity decays in Fig. 5. That is, neither represents the scale expected for a simple exponential decay. Even ignoring the initial spreading when $x < 0.1$, the shutdown of u^b is more rapid than either L or L^G suggests, indicating that arguments for shutdown length scales based solely on L or L^G may be misleading.

The cross-isobath structures of the bottom boundary layer and the interior velocity in the downstream equi-

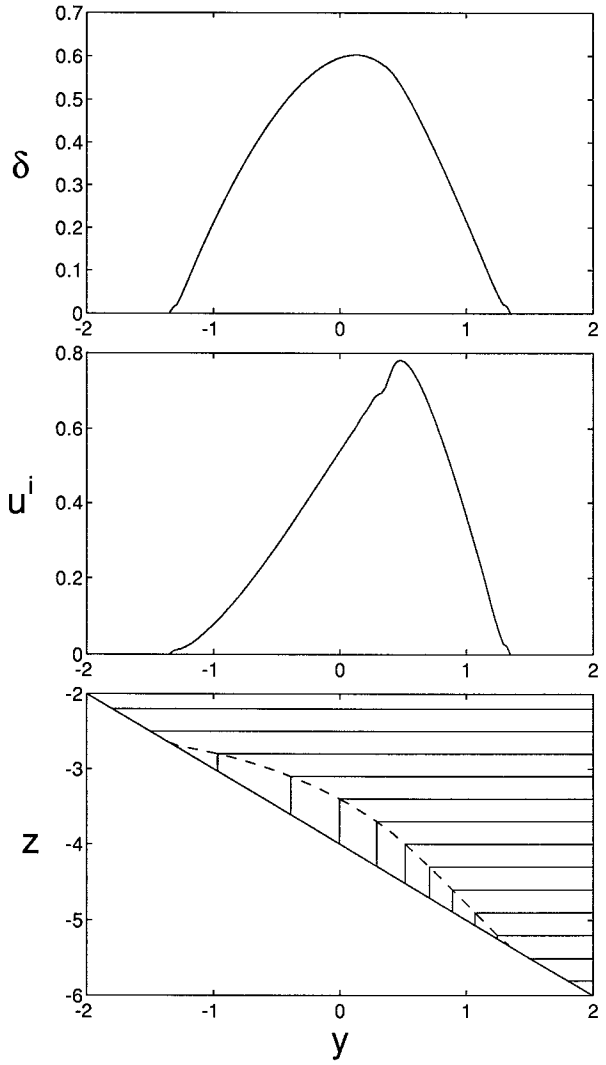

FIG. 7. Downstream equilibrium structure of (upper) bottom boundary layer thickness, (middle) interior along-isobath velocity, and (lower) density field at $x = 1$ for the stratified flow shown in Fig. 3.

librium ($x = 1$) are shown in Fig. 7. The boundary layer thickness is smooth and nearly symmetric about $y = 0$, while the interior velocity is asymmetric owing to the effects of stratification (also compare Figs. 3b and 4b). The along-isobath velocity is enhanced on the deeper side of the flow because the top of the bottom boundary layer slices through the interior density field at a steeper angle on that side of the flow, so the cross-isobath density gradient is greater there. This produces a larger vertical shear in the bottom boundary layer, which can support a larger interior velocity above the vanishing bottom velocity.

6. Downstream equilibrium

Three general constraints on the downstream equilibrium solution may be obtained by applying conservation of mass and buoyancy transport. These constraints are applicable for any inflow, and they may be applied to the special case of (20) to produce an approximate solution valid for any inflow width W_0. The discussion is again limited to the case of uniform stratification ($\Gamma' = 1$) over a uniformly sloping bottom ($h = h_0 + y$; $h_y = 1$), although it could be generalized further.

The model requires that the along-isobath flux of mass and buoyancy, integrated across the flow at any along-isobath (x) location, must equal the flux imposed at the inflow. Thus,

$$\int_{-Y_s}^{Y_d}\int_{-h}^{0} u\, dz\, dy = \int_{-\infty}^{\infty}\int_{-h}^{0} u_{in}(y)\, dz\, dy \tag{31}$$

$$\int_{-Y_s}^{Y_d}\int_{-h}^{0} u\rho\, dz\, dy = \int_{-\infty}^{\infty}\int_{-h}^{0} u_{in}(y)\rho|_{x=0}\, dz\, dy, \tag{32}$$

where the inflow velocity u_{in} is an arbitrary function of y that is spatially limited (i.e., $u_{in} \to 0$ as $y \to \pm\infty$), and $-Y_s$ and Y_d are, respectively, the shallow and deep edges of the current, defined as the positions at which the bottom boundary layer vanishes (i.e., $\delta = 0$ at $y = -Y_s$ and Y_d). For consistency with the scaling introduced in section 4, the inflow velocity must provide unit transport per unit depth; that is, $\int_{-\infty}^{\infty} u_{in}\, dy = 1$.

The interior flow is horizontally nondivergent with $w = 0$, so fluid never changes depth. This allows the vertical integrals on the left-hand side of (31) and (32) to be separated into two parts: an upper region above the shallowest depth of the bottom boundary layer, that is, $-h_0 + Y_s < z < 0$, and a lower region below this depth, that is, $-h < z < -h_0 + Y_s$. The velocities in the upper region are vertically uniform, so both (31) and (32) reduce to

$$\int_{-Y_s}^{Y_d} u^i\, dy = \int_{-\infty}^{\infty} u_{in}(y)\, dy = 1, \qquad -h_0 + Y_s < z < 0. \tag{33}$$

In the downstream equilibrium, both the velocity at the bottom and along-isobath variations in p^s must vanish (i.e., $u^b \to 0$ and $p^s_x \to 0$). From (26), boundary layer growth ceases, so both x-derivative terms in (25) disappear. Equation (25) may then be integrated to obtain

$$u^i = -p^s_y = (1 - \delta_y)\delta, \tag{34}$$

which is also obtained by setting $u^b = 0$ in (27). Substituting (34) into (33) and using the fact that $\delta = 0$ at $y = -Y_s$ and Y_d yields a constraint on the equilibrium flow:

Constraint 1

$$\int_{-Y_s}^{Y_d} \delta\, dy = \int_{-\infty}^{\infty} u_{in}(y)\, dy = 1. \tag{35}$$

Conservation of mass transport within the depth range spanned by the bottom boundary layer is imposed using

(31) but integrating vertically from the bottom to $z = -h_0 + Y_s$. Above the bottom boundary layer ($-h + \delta < z < -h_0 + Y_s$), the equilibrium velocity is again given by (34). Within the bottom boundary layer, the equilibrium velocity is given by (7) combined with (15), which in scaled form becomes

$$u = u^i - (1 - \delta_y)(\delta - h - z). \tag{36}$$

Using (34) and (36) in (31) and imposing constraint 1 leads to a second constraint on the equilibrium flow: constraint 2

$$\int_{-Y_s}^{Y_d} y\delta \, dy = \int_{-\infty}^{\infty} y u_{in}(y) \, dy. \tag{37}$$

Note that the right-hand side of (37) vanishes if the inflow is an even function, that is, if $u_{in}(-y) = u_{in}(y)$.

A third constraint is obtained from buoyancy conservation (32), applied within the depths spanned by the bottom boundary layer ($-h < z < -h_0 + Y_s$). The velocities above and within the bottom boundary layer are given by (34) and (36), respectively. The density above the bottom boundary layer is $\rho = -\rho_0 N^2 z/g$, while the density within the bottom boundary layer is given by (15) as $\rho^b = -\rho_0 N^2(\delta - h)/g$. Note that a density scale was not chosen in section 4, but the choice is unimportant here because it cancels when used in (32). Using these velocities and densities in (32) and imposing constraints 1 and 2, leads (after integration by parts and some algebra) to
constraint 3

$$\int_{-Y_s}^{Y_d} \left(y^2\delta - \frac{1}{3}\delta^3 \right) dy = \int_{-\infty}^{\infty} y^2 u_{in}(y) \, dy. \tag{38}$$

The above three constraints must be satisfied by the downstream equilibrium flow for any choice of inflow. Although they do not provide enough information to find a unique analytical solution, they can be used to derive a good approximate solution for the special case of a constant inflow $u_{in} = u_0$ over an inflow width $2W_0$ as defined by (20). In this case, the right-hand side of (37) vanishes, and the right-hand side of (38) equals $\frac{1}{3}W_0^2$.

In order to see the dependence of the downstream equilibrium structure on W_0, the basic calculation described in section 5 has been repeated for a wide range of inflow widths. In each case the inflow transport per unit depth is maintained at unity; that is, $2u_0W_0 = 1$. Examples of the downstream equilibrium are shown in Fig. 8 for several choices of W_0. The equilibrium width of the current increases with W_0, while the maximum height of the bottom boundary layer and the maximum velocity both decrease, as they must to maintain unit inflow. Spreading of the current takes place at the edges where the relative vorticity is largest.

For wide inflows, $W_0 > 2$, the adjustment is nearly two-dimensional (in the vertical and along-isobath directions). That is, the bulk of the inflow simply follows isobaths with the bottom boundary layer growing beneath. This flow is basically the analog of the one-dimensional models (e.g., Trowbridge and Lentz 1991) with along-isobath motion playing the role of time. The interior velocity hardly changes from its inflow value, and the bottom boundary layer simply grows thick enough to reduce the inflow velocity to zero at the bottom. Spreading is limited to smoothing at the edges, leaving a wide, flat region of constant boundary layer thickness and constant along-isobath velocity.

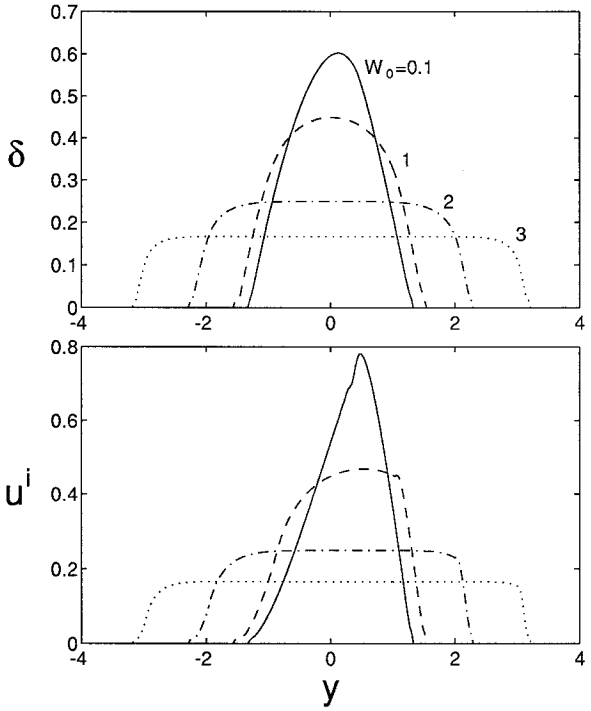

FIG. 8. Downstream equilibrium structure of (upper) bottom boundary layer thickness and (lower) interior along-isobath velocity for several choices of inflow width; $W_0 = 0.1$ (solid), 1 (dashed), 2 (dash–dotted), and 3 (dotted). Total inflow transport is unity in each case.

The simplest representation of the equilibrium bottom boundary layer thickness, which is consistent with the wide inflow results of Fig. 8, is a constant thickness δ_e from $y = -W_e$ to $y = W_e$ (i.e., $Y_s = Y_d = W_e$). This choice satisfies constraint 2 and is easy to use in the other constraints. Constraint 1 requires that $2\delta_e W_e = 1$, which can be combined with constraint 3 to find

$$W_e = \left[\frac{1}{2}W_0^2 + \frac{1}{2}(1 + W_0^4)^{1/2} \right]^{1/2}. \tag{39}$$

This estimate represents the effective width of the model downstream equilibrium if the boundary layer had uniform thickness. It can be compared to the model results by defining an effective model equilibrium width based on the maximum bottom boundary layer thickness δ_m; that is, $W_m = (2\delta_m)^{-1}$. This definition satisfies mass

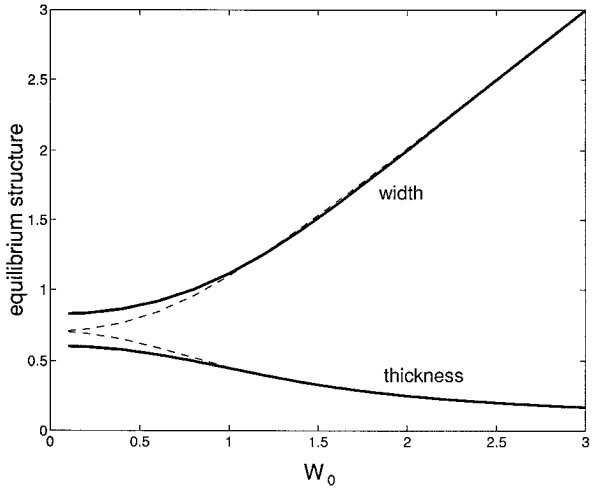

FIG. 9. Downstream equilibrium structure versus inflow width W_0. Solid curves are the maximum bottom boundary layer thickness δ_m (lower) and the effective current width $W_m = (2\delta_m)^{-1}$ (upper) from the model calculations. Dashed curves are the estimates based on a uniform boundary layer thickness δ_e and current width W_e in (39) combined with the equilibrium constraints (35), (37), and (38).

conservation for a constant boundary layer thickness of δ_m. Figure 9 shows W_m and δ_m as a function of inflow width (solid curves). The effective equilibrium width is fairly constant for narrow inflows ($W_0 < 0.5$) and then becomes nearly equal to W_0 for $W_0 > 1.5$. Estimates of equilibrium width W_e from (39) and boundary layer thickness $\delta_e = (2W_e)^{-1}$ are drawn as dashed curves in Fig. 9. Overall agreement is quite good. The largest discrepancies occur for narrow inflows ($W_0 < 1$) where the bottom boundary layer thickness is least like a constant. For $W_0 > 1$, the estimate is nearly identical to the model result. Thus, the three constraints derived above, based only on the downstream equilibrium, provide powerful restrictions on the solution, which may be used to approximate the equilibrium scales rather accurately.

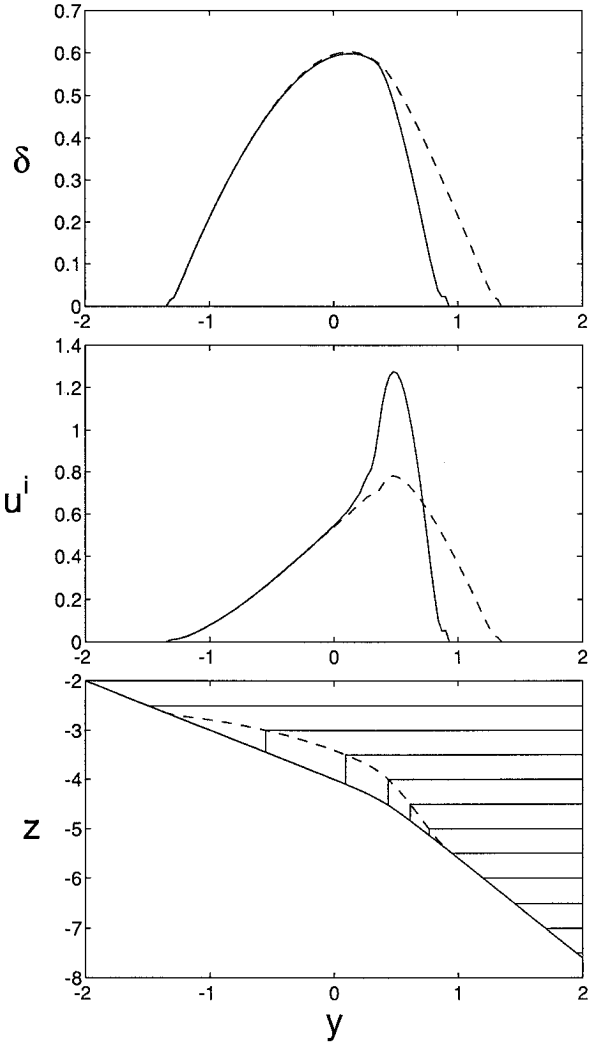

FIG. 10. As in Fig. 7 but for variable bottom slope (40) with $\alpha_1 = 1$, $\alpha_2 = 2$, $y_b = 0.4$, and $\Delta = 0.2$. Dashed curves are for a uniformly sloping bottom (Fig. 7).

7. Generalizations

For completeness, a few examples are presented here in which the simplifications of a uniformly sloping bottom and uniform stratification are relaxed. In addition, flows adjacent to a coastal boundary are considered briefly. In all cases, the basic behavior is fairly easy to understand based on results from the previous sections.

a. Variable bottom slope

According to (29), the cross-isobath adjustment scale (for a narrow inflow) is inversely proportional to the bottom slope, so an inflow spreads across the isobaths more (less) over a gentler (steeper) bottom slope. Therefore, an inflow that encounters a change in bottom slope is expected to remain narrower over the steeper part of the topography. To demonstrate, the adjustment of the narrow inflow of section 5 has been calculated over variable bottom slope by solving (25)–(28) with bottom slope h_y varying smoothly in y from α_1 to α_2 as

$$h_y = \frac{1}{2}(\alpha_1 + \alpha_2) + \frac{1}{2}(\alpha_2 - \alpha_1)\tanh[(y - y_b)/\Delta], \tag{40}$$

where y_b is the location of the change in bottom slope, and Δ is the scale over which the slope changes. Uniform stratification is assumed as before, $\Gamma' = 1$.

Figure 10 shows the downstream equilibrium achieved with $\alpha_1 = 1$, $\alpha_2 = 2$, $y_b = 0.4$, and $\Delta = 0.2$. The change in bottom slope occurs on the deeper side of the inflow, but within the adjustment scale for the uniform slope (i.e., $y_b < 1$). As the inflow spreads, most of the flow encounters the same slope as in section 5, but some of the deeper part of the flow must adjust to

the steeper bottom slope. Thus, the inflow widens nearly identically to Fig. 3 until the deeper part encounters the steeper bottom slope. The shallower part then continues as before, while the deeper part spreads less. Not surprisingly, the boundary layer thickness and along-isobath velocity over the gentler slope are nearly identical to those in Fig. 7. Over the steeper slope, the width of the equilibrium flow is roughly halved, while the maximum velocity is approximately doubled, and the maximum boundary layer thickness is nearly unchanged. These changes are all consistent with (24) and (29). The result is a strong, narrow jet near the break in topography.

b. *Variable stratification*

Variations in the interior stratification affect the adjustment of the inflow by changing the horizontal density gradients within the bottom boundary layer, which in turn alter the vertical shear [see (11)]. Where relatively stronger (weaker) stratification occurs at the top of the bottom boundary layer, the vertical shear within the boundary layer is larger (smaller), so a given bottom boundary layer thickness will reduce a larger (smaller) interior velocity to zero at the bottom. Alternatively, a thinner (thicker) bottom boundary layer beneath stronger (weaker) stratification is required to reduce a given interior velocity to zero at the bottom. Thus, regions of stronger (weaker) stratification should correspond to regions of stronger (weaker) equilibrium interior currents and/or thinner (thicker) bottom boundary layers. This behavior may be demonstrated by solving (25)–(28) as before over a uniformly sloping bottom, but now allowing variable background stratification. As a byproduct, the depth now enters the problem because the stratification varies with height above the bottom. Therefore, some depth must be specified, so the x axis ($y = 0$) is chosen to coincide with the $h = 4$ isobath.

Figure 11 shows the equilibrium flow structure for exponential background density profiles of the form

$$\Gamma(z) = \gamma(e^{z/\gamma} - 1). \tag{41}$$

Uniform stratification corresponds to $\gamma \to \infty$. Any finite choice for γ corresponds to decreasing stratification with depth. As anticipated, decreased stratification leads to a broader and weaker equilibrium flow with a thicker bottom boundary layer. The changes are more pronounced on the deeper side of the flow where the stratification is weakest.

Local changes in background stratification, for example, a pycnocline, may also dramatically affect the equilibrium flow. Figure 12 shows the equilibrium flow in the presence of a density profile with a pycnocline at $z = -z_0$;

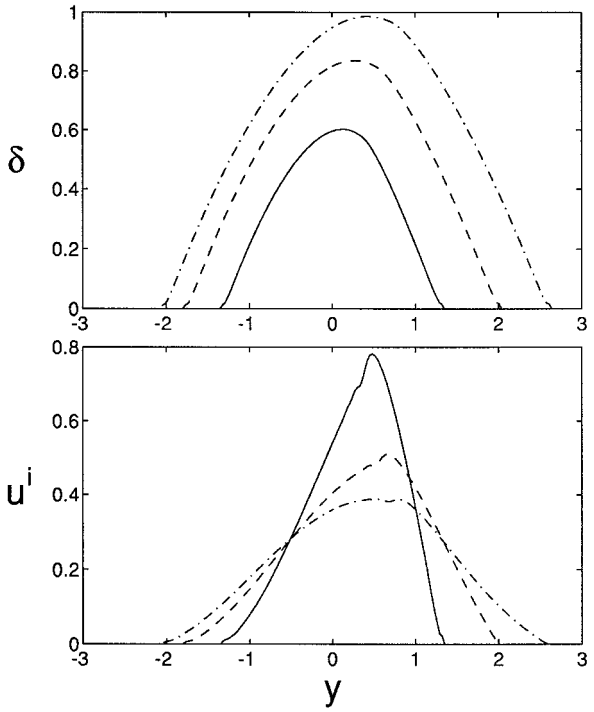

FIG. 11. Downstream equilibrium structure of (upper) bottom boundary layer thickness, and (lower) interior along-isobath velocity at $x = 1$ for exponential stratifications given by (41) with $\gamma = \infty$ (uniform stratification as in Fig. 7; solid), $\gamma = 5$ (dashed), and $\gamma = 3$ (dash-dotted).

$$\Gamma(z) = \left[1 - \beta \operatorname{sech}^2\left(\frac{z_0}{\Delta z}\right)\right] z + \beta \Delta z \left[\tanh\left(\frac{z + z_0}{\Delta z}\right) - \tanh\left(\frac{z_0}{\Delta z}\right)\right], \tag{42}$$

where β represents the local increase in buoyancy frequency at the pycnocline and Δz is the thickness of the pycnocline. The pycnocline in Fig. 12 ($z_0 = 4$, $\Delta z = 0.25$, $\beta = 2$) intersects the top of the bottom boundary layer on the deeper side of the equilibrium flow. The horizontal density gradients within the boundary layer are locally increased, thereby increasing the vertical shear. As a result, a stronger interior velocity is maintained in this region over a thinner bottom boundary layer. The shallower part of the equilibrium flow is largely unaltered by the pycnocline, but the deeper flow is reduced because that transport is carried by the strong, narrow jet generated at the pycnocline. The net effect is similar to the change in bottom slope shown in Fig. 10.

c. *Coastal currents*

The present model may be used to examine the adjustment and evolution of an inflow in the presence of a coastal boundary by applying boundary condition

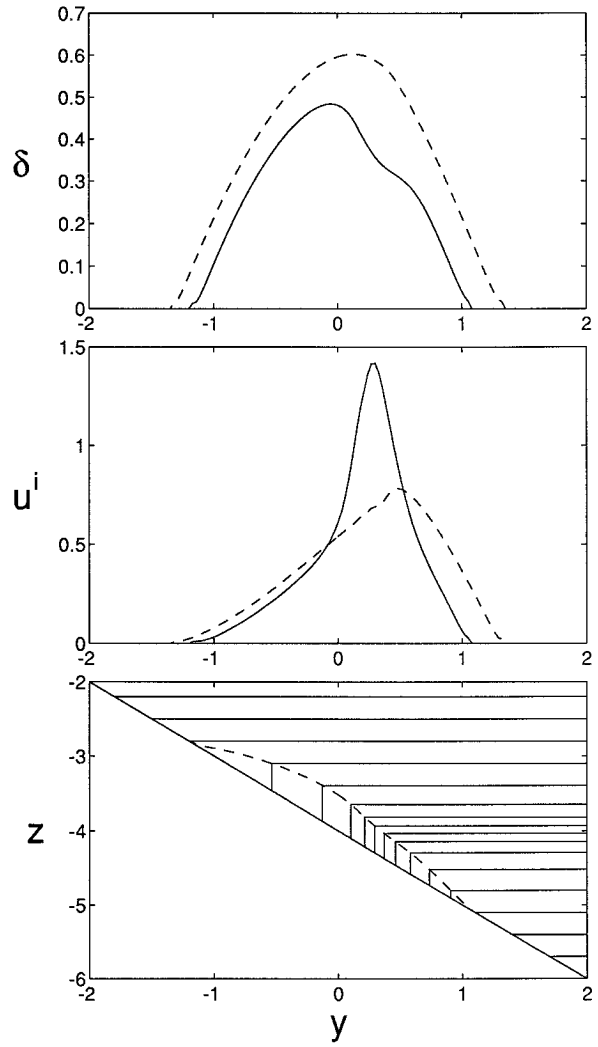

FIG. 12. As in Fig. 7 but for pycnocline stratification given by (42) with $z_0 = 4$, $\Delta z = 0.25$, and $\beta = 2$. Dashed curves are for uniform stratification (Fig. 7).

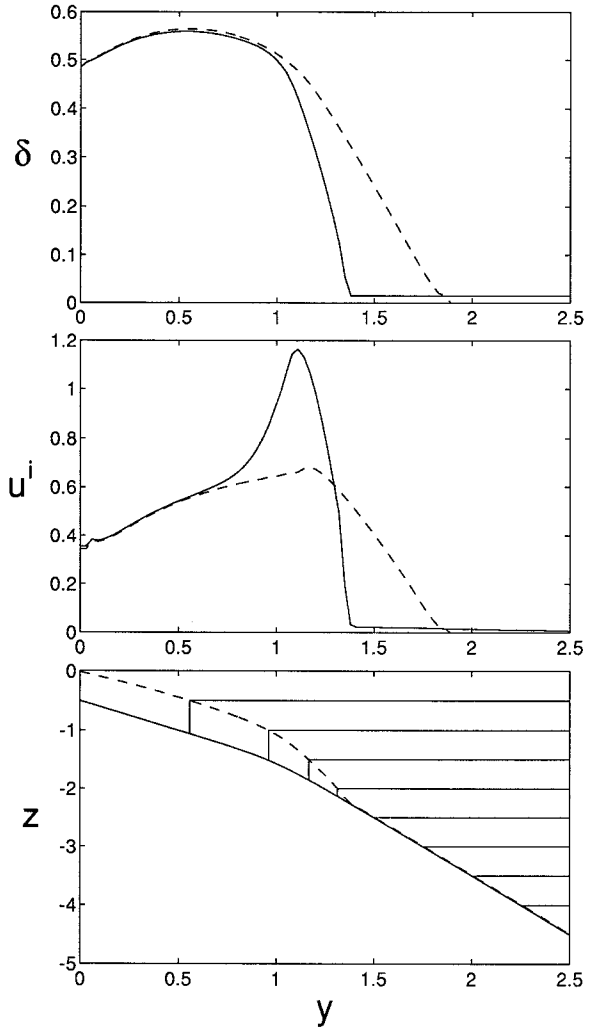

FIG. 13. As in Fig. 7 but for a flow bounded by a coastal wall of depth $h_c = 0.5$ located at $y = 0$ and depth given by (43) with $\alpha_1 = 1$, $\alpha_2 = 2$, $y_b = 1$, and $\Delta = 0.2$. Dashed curves correspond to the same case but with a uniformly sloping bottom, $\alpha_1 = \alpha_2 = 1$.

(22). The coastal boundary restricts the spreading of the inflow such that it may move only into deeper water. Typical results are shown in Fig. 13 for an inflow with width $W_0 = 1$ and velocity $u_0 = 1$ adjacent to the coast ($y = 0$). Stratification is uniform, $\Gamma'(z) = 1$. The scaled bottom topography has the form

$$h = h_c + \frac{1}{2}(\alpha_1 + \alpha_2)y + \frac{\Delta}{2}(\alpha_2 - \alpha_1) \times \left\{ \ln\left[\cosh\left(\frac{y - y_b}{\Delta}\right)\right] - \ln\left[\cosh\left(\frac{y_b}{\Delta}\right)\right] \right\}, \quad (43)$$

which has depth h_c at $y = 0$, and the slope h_y is given by (40). The dashed curves correspond to the equilibrium flow over a uniformly sloping bottom ($\alpha_1 = \alpha_2 = 1$ and $h_c = 0.5$). The solid curves and the lower panel correspond to a change in bottom slope at $y = 1$, similar to a shelf break although not very sharp ($\alpha_1 = 1$, $\alpha_2 = 2$, $y_b = 1$, $\Delta = 0.2$, and $h_c = 0.5$). In both cases, the current spreads into deeper water and reaches an equilibrium with the strongest currents near the outer edge of the flow. The maximum boundary layer thickness is slightly greater and the equilibrium width wider than the noncoastal case with $W_0 = 1$ because more transport is forced to move into the deeper water in the coastal case. The effect of the shelf break is qualitatively identical to that in Fig. 10; a strong and narrow jet (approaching twice the maximum speed) forms near the change in bottom slope. The implication is that the shelf break acts somewhat like a barrier, inhibiting the coastal current from simply moving offshore over the continental slope.

In both cases shown in Fig. 13, the bottom boundary layer just reaches the surface at the coast. The effect of

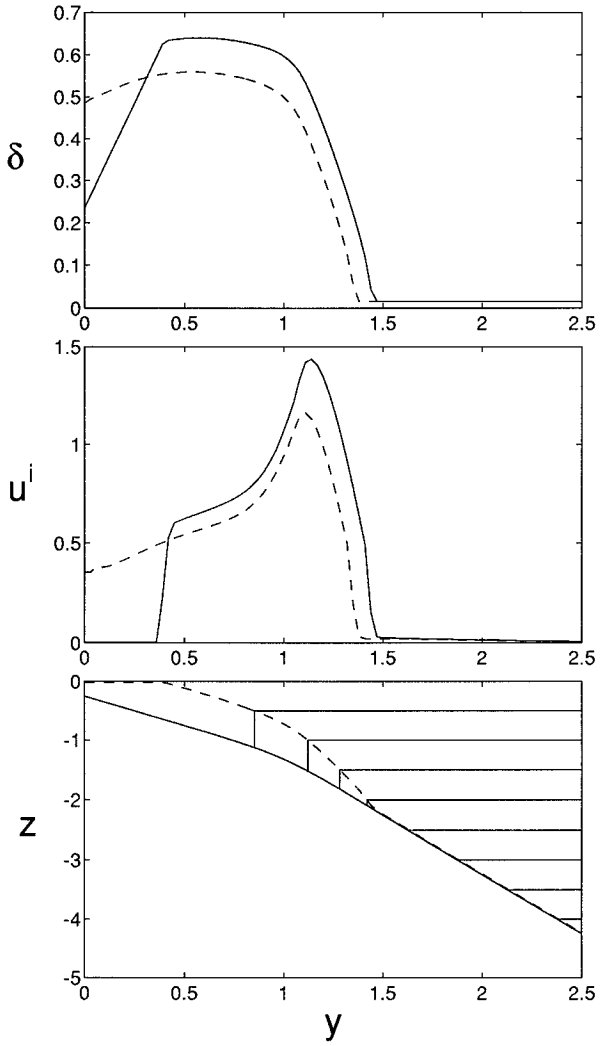

FIG. 14. As in Fig. 13 but for a shallower coastal wall; $h_c = 0.25$. Dashed curves are for the deeper coastal wall (solid curves in Fig. 13).

this on the equilibrium flow is minimal. If the coastal depth is reduced to $h_c = 0.25$ while maintaining unit inflow, then the bottom boundary layer reaches the surface over a large portion of the shelf ($y \lesssim 0.4$). The horizontal density gradients vanish in this region, and so must the vertical shear. Therefore, the interior velocity must match the bottom velocity, which is zero in the equilibrium flow. As a result, the equilibrium flow (Fig. 14) moves offshore leaving a stagnant region adjacent to the coast. Further, the increased transport near the change in bottom slope generates a stronger and slightly wider jet compared to the previous case with a deeper coastal boundary (dashed curves).

8. Discussion

The model constructed here, despite its many idealizations, provides insight into the general behavior of stratified ocean flows over a sloping bottom. In particular, the model demonstrates the importance of both density advection in the bottom boundary layer and, especially, feedback between the boundary layer and the overlying flow, thereby progressing beyond one-dimensional models of bottom boundary layer growth in which the overlying flow that drives the bottom boundary layer is fixed at its initial value. In addition, the scaling (24) eliminates all free parameters, so the insights may be applied to many situations. The present model also allows the investigation of spatially varying currents over variable bottom topography in the presence of variable stratification in a straightforward way. The existence of a downstream equilibrium in which bottom stress vanishes everywhere provides a mechanism for narrow ocean currents to persist over long distances with little change in structure or properties. This contrasts with the model proposed by MacCready (1994) that explains long ocean currents by appealing to the gradual drainage of fluid and energy by bottom Ekman transport; if the drainage is slow enough, then the current persists for a long distance before spinning down. In the present model, however, there is no drainage or spin down at all, once the downstream equilibrium is reached, so the current persists indefinitely!

The present model results also suggest that the horizontal (cross isobath) structure of persistent ocean currents (i.e., having reached an equilibrium) may be largely determined by the dynamics of the underlying bottom boundary layer. In regions of uniform bottom slope, currents should be stronger on the deeper side of the flow. Over variable topography with nonuniform stratification, currents should be strongest where the bottom slope is greatest and where the interior stratification is strongest. Remarkably, and in contrast to one-dimensional models, the thickness scale of the bottom boundary layer is independent of the bottom slope, reaching a finite size even over a very gentle slope (e.g., over the continental shelf). Further, the model equilibrium flow is independent of the magnitude of bottom friction, suggesting that the precise form assumed for bottom stress may not be important, so the model results may apply more generally than originally anticipated.

The model results also have implications concerning the formation of shelfbreak fronts. Wright (1989) proposed that a shelfbreak front can form as a shelf front, which separates fresher water from denser water, and is moved offshore by bottom Ekman transport until it reaches the shelf break. Chapman and Lentz (1994) showed that this may not work because the front may reach an equilibrium position where it stops moving offshore, similar to the present situation. The present results suggest that whether or not bottom Ekman transport can carry a coastal flow to the shelf break depends on the relative size of W from (29) and the shelf width. If the source flow is initially narrow compared with W and the shelf is wider than about $2W$, then the flow should not reach the shelf break. Instead, a midshelf

front may form. If the shelf width is less than $2W$, then an initially narrow flow should reach the shelf break where the change in bottom slope should impede further progress offshore (e.g., Fig. 10). This situation is consistent with the formation mechanism proposed by Gawarkiewicz and Chapman (1992). They showed that a front forms at the shelf break where the spreading coastal flow encounters the change in bottom slope causing the bottom boundary layer to detach from the bottom.

One significant difference between the present model and that of Gawarkiewicz and Chapman (1992) is that a surface-to-bottom front does not form near the shelf break in the present model (see Figs. 13 and 14). This occurs because the interior of the present model is assumed inviscid, whereas Gawarkiewicz and Chapman (1992) used a constant vertical mixing coefficient throughout the water column. Indeed, numerical model calculations identical to those of Gawarkiewicz and Chapman (1992), but with greatly reduced vertical mixing outside the bottom boundary layer, produce flows very much like those in Figs. 13 and 14. These, and other related results, will be reported separately.

Many simplifications and assumptions were made in constructing the present model, thus making it difficult to apply the results directly to observed ocean currents. For example, the model interior flow is vertically uniform with no vertical shear of the horizontal currents and no sloping isopycnals. Bottom-intensified flows, such as poleward undercurrents and deep western boundary currents, do not generally have these properties. The model topography is assumed to vary only in one direction, so regions of complex bathymetry are not properly modeled. The model only allows the boundary layer to grow or equilibrate but never to shrink because there is no way to restratify the water column. So, upwelling-favorable flows and/or rapidly decelerating flows cannot be modeled. Furthermore, the dynamics of the model bottom boundary layer are particularly simple, ignoring shear generated by inertial oscillations and that within the log-layer near the bottom.

Another limitation of the present model is the assumption that the bottom boundary layer must remain attached to the bottom, which may not be the case in some flows. For example, if convergence within the bottom boundary layer becomes strong enough, then large vertical velocities can be generated that cause the bottom boundary layer to detach from the bottom and thereby modify the interior flow (e.g., Gawarkiewicz and Chapman 1992; Chapman and Lentz 1994). The present model responds to strong convergences, such as a change in bottom slope, by turning the flow along the isobaths, forming a narrow along-isobath jet (Fig. 10). A related issue is that the jet may become so strong and narrow that it is unstable to small perturbations; that is, the neglect of nonlinear advection in the momentum equations becomes questionable. Resolution of these issues probably requires comparison of the present model results with similar calulations using a sophisticated numerical model and is not attempted here.

Regardless of the model limitations, estimates of model scales for various oceanic conditions can be made that establish the relevance of the model results. For example, recent observations of the deep western boundary current south of the Grand Banks at 55°W show the transport to be about 15×10^6 m^3 s^{-1} with a vertical scale of about 2000 m, a horizontal width of 150–200 km, and geostrophic velocities between 0.03 and 0.09 m s^{-1} (R. Pickart 1995, personal communication). Taking $F_0 = (15 \times 10^6/2000)$ m^2 s^{-1}, $\alpha = 10^{-2}$, $N = 10^{-3}$ s^{-1}, and $f = 10^{-4}$ s^{-1} in (29) yields $W = 87$ km. From (24), the along-isobath velocity scale is 0.087 m s^{-1}, while the boundary layer thickness scale is 866 m. Based on the narrow inflow results and the downstream equilibrium calculations (i.e., using the precise values from Fig. 7), the equilibrium flow would have a total width of $2 \times 1.32W = 229$ km with an along-isobath velocity maximum of about 0.067 m s^{-1} and maximum boundary layer thickness of about 520 m; all quite reasonable compared with Pickart's recent observations.

Another example is the shelf flow along the Middle Atlantic Bight. Here the transport is roughly 0.5×10^6 m^3 s^{-1} distributed over an average depth of about 70 m (e.g., Beardsley et al. 1985). Taking $\alpha = 10^{-3}$, $N = 10^{-2}$ s^{-1}, and $f = 10^{-4}$ s^{-1} leads to $W = 85$ km. The along-isobath velocity scale is 0.085 m s^{-1} while the bottom boundary layer thickness scale is 85 m. Using the results shown in Fig. 13 for the uniformly sloping bottom, the equilibrium flow would have a total width of about 150 km. The width is wider than the shelf, consistent with the existence of a shelfbreak front in the Middle Atlantic Bight. The peak velocity is about 0.058 m s^{-1}, and the maximum boundary layer thickness is about 48 m. All of these values are again quite reasonable, suggesting that the present model may provide insight for a variety of situations.

The final point of discussion concerns the neglect of the contribution of the interior cross-isobath velocity to the cross-isobath buoyancy flux in the bottom boundary layer in going from (13) to (14). The scaling (24) shows that the omitted term $\delta f v^i$ is, in fact, the same order as ru^b, so its neglect is not strictly valid. Nevertheless, this term is omitted for the following reason: The inflow is purposely chosen to be out of dynamical balance in order to study the downstream adjustment of the flow. The interior cross-isobath velocity just downstream of the inflow is, therefore, exceptionally large at the edges of the inflow. In fact, it violates the model assumption that $v^i \ll u^i$, so the transport in the bottom boundary layer would be dominated by v^i if it were included. The adjustment process of interest would be overwhelmed by this term. The implicit assumption is that other processes, also neglected, would rapidly reduce the cross-isobath velocity near the inflow, so its influence on the

development of the downstream equilibrium would be unimportant.

To determine whether or not neglecting this term substantially alters the model results, calculations have been made using a primitive-equation numerical model configured to represent the narrow inflow reported in section 5 and the coastal current described in section 7c. In both cases, the primitive equation model produces an adjustment of the inflow much like that described here and reaches a downstream equilibrium that is both qualitatively and quantitatively similar to the idealized model results. There are some differences in the details, of course, but it is clear that the idealized model captures the essence of the adjustment process quite well. In particular, the interior cross-isobath velocity is rapidly reduced near the inflow and is unimportant in the flow adjustment. The numerical model also provides more details of the flow, for example, the velocity structure within the bottom boundary layer, and the results of a more comprehensive study will be reported separately.

Some additional confidence in the present model results comes from the good agreement between the model results and the estimate of the downstream equilibrium (Fig. 9). The estimate is based only on the constraints derived in section 6 and a very simple form for the bottom boundary layer thickness (a constant). The constraints were developed independent of the details of the adjustment process, so the neglect of the cross-isobath velocity term in (13) is not an issue. The close agreement in Fig. 9 suggests that the model reaches the correct downstream equilibrium. To test this further, other shapes for the narrow inflow were imposed instead of (20), and in all cases the downstream equilibrium structure was nearly identical to that shown in Fig. 7, again supporting the simplified dynamics assumed here.

9. Conclusions

The adjustment of stratified along-isobath flow over a sloping, frictional bottom has been examined using an idealized model in which the feedback between the bottom boundary layer and the overlying flow plays a crucial role. That is, the overlying flow that drives the bottom boundary layer flow is itself altered by the evolving flow in the boundary layer. The typical sequence of events is as follows: A vertically uniform inflow of limited spatial extent generates a bottom boundary layer that transports water downslope. The downslope advection of density creates horizontal density gradients within the boundary layer that produce vertical shears of the along-isobath velocity beneath the overlying flow. The shears reduce the velocity at the bottom and, therefore, the bottom stress. This, in turn, alters the boundary layer transport, which thereby changes the overlying flow. Eventually, an equilibrium is reached downstream in which the bottom velocity is zero everywhere and the overlying flow ceases to adjust. The equilibrium flow then persists indefinitely, despite the presence of a frictional bottom.

The equilibrium flow formed by a narrow inflow over a uniformly sloping bottom with initially uniform stratification has a cross-isobath adjustment scale of $W = (f/N\alpha)(F_0/f)^{1/2}$ where f is the Coriolis parameter, N the buoyancy frequency, α the bottom slope, and F_0 the inflow volume flux per unit depth. The thickness of the bottom boundary layer scales as αW, while the along-isobath velocity scales as $(N\alpha/f)(F_0 f)^{1/2}$. Somewhat surprisingly, the downstream equilibrium flow is independent of the magnitude of bottom friction, although the along-isobath distance required to reach equilibrium is inversely proportional to the bottom friction coefficient r. These scales are useful for understanding generalizations of the model to variable bottom slopes, nonuniform stratification, and coastal currents. Conservation properties provide a means of approximating the downstream equilibrium structure for an inflow with arbitrary width.

Acknowledgments. We are indebted to Chris Garrett for several valuable comments and suggestions that he made following a presentation of this work in June of 1995 in Woods Hole. We thank Bob Pickart for generously sharing his preliminary estimates of deep western boundary current properties. Financial support for DCC was provided by an Independent Study Award from the Woods Hole Oceanographic Institution, as well as the National Science Foundation (NSF) under Grants OPP-9113940, OPP-9422292, and OCE-9415484. Financial support for SJL was provided by NSF under Grant OCE-9221615 and the Coastal Science Program of the Office of Naval Research under Grant N00014-89-J-1074.

REFERENCES

Beardsley, R. C., D. C. Chapman, K. H. Brink, S. R. Ramp, and R. Schlitz, 1985: The Nantucket Shoals Flux Experiment (NSFE79). Part I: A basic description of the current and temperature variability. *J. Phys. Oceanogr.*, **15,** 713–748.

Chapman, D. C., and S. J. Lentz, 1994: Trapping of a coastal density front by the bottom boundary layer. *J. Phys. Oceanogr.*, **24,** 1464–1479.

Csanady, G. T., 1978: The arrested topographic wave. *J. Phys. Oceanogr.*, **8,** 47–62.

Garrett, C., P. MacCready, and P. Rhines, 1993: Boundary mixing and arrested Ekman layers: Rotating stratified flow near a sloping boundary. *Annu. Rev. Fluid Mech.*, **25,** 291–323.

Gawarkiewicz, G., and D. C. Chapman, 1992: The role of stratification in the formation and maintenance of shelfbreak fronts. *J. Phys. Oceanogr.*, **22,** 753–772.

MacCready, P., 1994: Frictional decay of abyssal boundary currents. *J. Mar. Res.*, **52,** 197–217.

——, and P. B. Rhines, 1993. Slippery bottom boundary layers on a slope. *J. Phys. Oceanogr.*, **23,** 5–22.

Trowbridge, J. H., and S. J. Lentz, 1991: Asymmetric behavior of an oceanic boundary layer above a sloping bottom. *J. Phys. Oceanogr.*, **21,** 1171–1185.

Wright, D. G., 1989: On the alongshelf evolution of an idealized density front. *J. Phys. Oceanogr.*, **19,** 532–541.